

Charge Fluctuations and the Valence Transition in Yb under Pressure

E. R. Ylvisaker,¹ J. Kuneš,^{2,3} A. K. M. M. Ahan,⁴ and W. E. Pickett¹

¹Department of Physics, University of California, Davis, California, 95616

²Theoretical Physics III, Center for Electronic Correlations and Magnetism, Institute of Physics, University of Augsburg, Augsburg 86135, Germany

³Institute of Physics, Academy of Sciences of the Czech Republic, Cukrovarnicka 10, 162 53 Praha 6, Czech Republic

⁴Lawrence Livermore National Laboratory, Livermore, California 94550-9234, USA

(dated: April 2, 2024)

We present a dynamical mean-field theory study of the valence transition ($f^{14} \rightarrow f^{13}$) in elemental, metallic Yb under pressure. Our calculations reproduce the observed valence transition as reflected in the volume dependence of the 4f occupation. The transition is accelerated by heating, and suggests quasiparticle or Kondo-like structure in the spectra of the trivalent end state, consistent with the early lanthanides. Results for the local charge fluctuations and susceptibility, however, show novel signatures uniquely associated with the valence transition itself, indicating that Yb is a fluctuating valence material in contrast to the intermediate valence behavior seen in the early trivalent lanthanides Ce, Pr, and Nd.

PACS numbers: 71.20.Eh, 74.40.+k, 75.20.Hr

The valence state of rare earth atoms in lanthanide compounds has a crucial effect on their physical properties. Determination of the lanthanide valence from first principles and description of the 4f electrons has been a long standing challenge due to the duality between their atomic character, stemming from the on-site electron-electron interaction, and the itinerant character, due to the lattice periodicity. Theories based on the two species picture, which treat part of the 4f electrons as atomic and the rest as itinerant, succeeded in reproducing the trends across the lanthanide series for compounds with integer valence [1]. Nevertheless, besides being conceptually unsatisfactory, the two species picture cannot describe transitions between different valence states as well as such outstanding behavior as heavy fermions. Only recently has the combination (LDA + DMFT) [2, 3] of the local-density approximation (LDA) and dynamical mean-field theory (DMFT) been applied to the rare earth materials [4, 5, 6, 7, 8, 9], providing a material specific electronic structure including the local many-body dynamics.

In this Letter we employ the LDA + DMFT method to study the valence transition and charge fluctuations in elemental Yb metal. It is well known that Yb and Eu behave differently from the other lanthanides in their elemental form. If we define the valence state as the number of electrons participating in bonding, the majority of the lanthanide series is trivalent, however for Yb and Eu the 3+ and 2+ valence states are close to degenerate with 2+ state being more stable at ambient conditions [1]. This results in a number of anomalous properties, such as a larger molar volume (as compared to the trend the rest of the lanthanide series follows), a lower bulk modulus [10], and the thermal expansion coefficient of Yb being three times larger than for most other lanthanides [11]. The gradual transition from the divalent to the trivalent state occurs in Yb over the range 0–34 GPa,

where the full 4f shell is opened as an f electron is promoted to the valence band. The doped 4f holes can move through the crystal by thermally activated hopping with spd bands acting as particle and energy reservoirs, fluctuating valence behavior, or they can move coherently between atomic sites forming a narrow band well known for heavy fermions, intermediate valence behavior. We will discuss how these concepts apply to Yb.

In the present study we start with a self-consistent LDA calculation, transform its one-electron Hamiltonian into an orthogonal Wannier function basis, H_k^{LDA} , and then calculate the 4f interaction parameter U as well as the the double counting correction to H_k^{LDA} . Since the valence transition of Yb is of principal interest here, we have to retain the 6s, 6p, and 5d valence orbitals to allow changes of the f-shell occupation. We assume the $SU(N)$ symmetric form of the local interaction

$$H_{\text{int}} = \frac{1}{2} U \sum_{i \neq j} \hat{n}_f^i \hat{n}_f^j; \quad (1)$$

(the interaction parameter U is a function of the specific volume is shown in the inset of Fig. 1), and express the local Green's function in the relativistic $j = 5=2, 7=2$ basis to make the off-diagonal elements small so that they can be neglected. To solve the auxiliary impurity problem we employ two Quantum Monte Carlo (QMC) solvers, one using the Hirsch-Fye (HFQMC) [12] algorithm and the other using the hybridization expansion continuous time QMC algorithm (CTQMC) [13] as well as an approximate, but computationally efficient Hubbard-I (HI) solver. Extrapolations of the HFQMC results to an infinite number of imaginary time slices were found to agree within statistical uncertainties with the CTQMC. However, we point out that especially at the larger L values, the HFQMC calculations had significant difficulties with ergodicity in the midst of the Yb valence transition where large fluctuations in

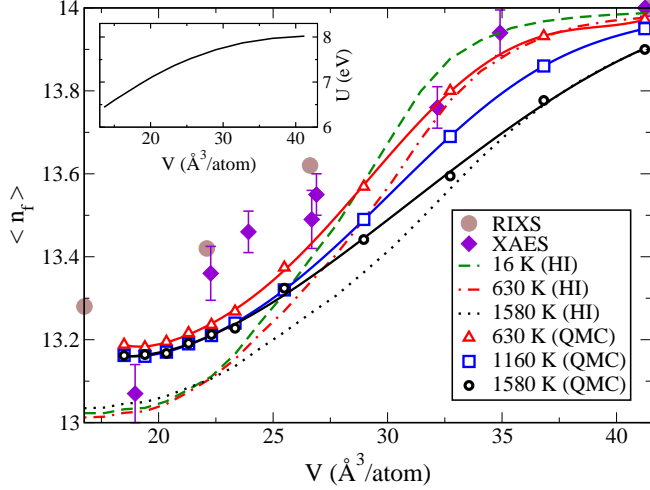


FIG. 1: (Color online) The f shell occupation vs pressure at various temperatures compared to the experimental data (closed symbols). Open symbols are QMC data; the 630 K and 1160 K curves were obtained with CTQMC, and the 1580 K curve with HFQMC at $L = 80$. The consistency of HFQMC with the CTQMC data was checked by $L = 1$ extrapolation of the $L = 80, 112$ and 160 data at 630 K. X-ray absorption edge spectroscopy (XAES) data was taken from Ref. 15, and resonant inelastic x-ray scattering (RIXS) data taken from Ref. 16. Inset shows the interaction U vs. specific volume.

n_f were encountered in the Ising space sampling. The CTQMC method did not encounter such problems, nor did HFQMC without any valence transition (e.g., Ce, Pr, and Nd [7, 14]).

In Fig. 1 we show the evolution of the f -orbital occupation n_f as a function of the specific volume V at various temperatures. Comparison to the experimental x-ray absorption edge spectroscopy (XAES) and resonant inelastic x-ray spectroscopy (RIXS) data shows some underestimation of n_f at lower volumes, possibly originating from the lack of charge self-consistency, which would take into account the correlation driven redistribution of charge between the f and spd orbitals. Overall the DMFT (QMC) results agree reasonably well with the experimental data over the entire pressure range of interest. Note that the rising $6s$ and $6p$ bands lead to an increase in n_f with compression for the trivalent rare earths [7], so that it is likely that the plateau in the DMFT (QMC) value reached at the smallest volumes in Fig. 1 is indeed near the end of the transition from divalent to trivalent in spite of the fact that n_f is still larger than 13.0. The ability of DMFT (HI) to produce the valence transition seen in experiment suggests that the physics is essentially related to charge transfer between the f and spd orbitals. At smaller volumes where delocalization of f -electrons becomes more important HI overestimates the number of holes in the $4f$ shells.

The calculated n_f values show a sizable temperature dependence both with HI and QMC, particularly at low

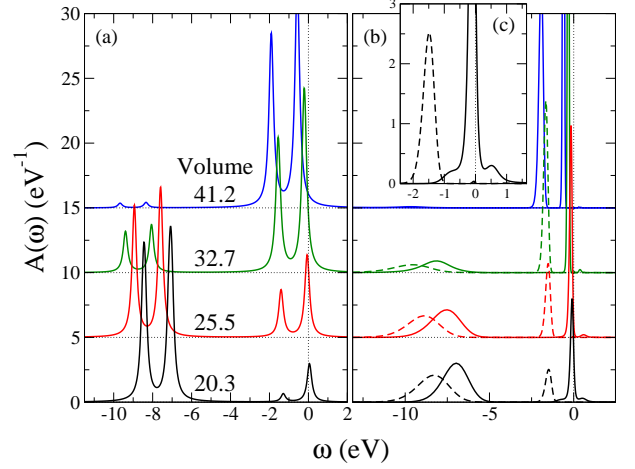


FIG. 2: (Color online) Plot of Yb spectral function $A(\omega)$ calculated in (a) HI at $T = 630$ K and (b) CTQMC at $T = 1160$ K for selected volumes (in $\text{\AA}^3/\text{atom}$). Dashed curves in (b) are for $j = \frac{5}{2}$; solid curves, $j = \frac{7}{2}$. Spin-orbit split peaks corresponding to the $f^{14} \rightarrow f^{13}$ excitation are near the chemical potential, while those corresponding to the $f^{13} \rightarrow f^{12}$ excitation are around $U(V)$. An expanded view near the Fermi level for $V = 20.3 \text{ \AA}^3/\text{atom}$ is shown in (c). The $j = \frac{7}{2}$ curve shows two shoulders around the large central peak.

pressure as is evident in Fig. 1. The general trend is that at higher temperatures, the f^{13} state is favored over the f^{14} state. This trend can be followed down to the lowest studied temperature of 16 K, which is only accessible with HI. We expect this trend would hold at lower temperatures for QMC calculations as well. Temperature dependent measurements of the valence of Yb in YbInCu_4 show the same trend (4f occupation decreasing with increasing temperature) [17], with different studies finding a minimum of about 13.1 [18, 19]. The same behavior was found for YbAgCu_4 and YbAl_3 [20]. The authors of Ref. 20 did not find any significant difference in elemental Yb between the temperatures of 250 K and 25 K; at 250 K Yb should be already strongly divalent and lowering the temperature cannot decrease the valence any further. There is, however, a significant broadening of the spectrum at higher temperature, so we expect that the trend seen in our calculations would be borne out if measurements were carried out at higher temperatures. At high pressure the temperature dependence of n_f becomes weak. The chemical environment of Yb can affect the temperature sensitivity of n_f as well; in fact, the measured valence of Yb in YbGaGe has been recently found to be temperature independent [21], and Yb nearly divalent. This is somewhat a contrast to our result here, where the temperature sensitivity is only near the divalent state. The details of the electronic structure of YbGaGe that causes the Yb valence to be temperature independent are not understood.

The calculated $4f$ spectral densities $A(\omega)$ are shown in Fig. 2, as obtained by direct evaluation of the Green's

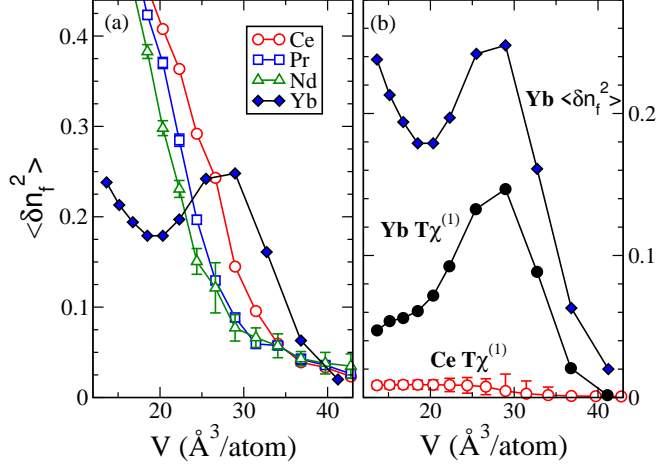


FIG. 3: (Color online) (a) Equal time charge fluctuations in Yb (CTQMC), Ce, Pr and Nd (HFQMC with $L = 1$ extrapolation) at 630 K. If not shown error bars are smaller than the symbol size. (b) Charge fluctuations for Yb (diamonds, the same as in left panel) compared to their imaginary time average, $T^{(1)}$, for Yb (closed circles) and Ce (open circles).

function near the real frequency axis for HI, and applying the maximum entropy method [22] to the CTQMC data. At low pressure, there is a clear spin-orbit-split peak near the chemical potential ($\mu = 0$), which corresponds to the $f^{14} \rightarrow f^{13}$ excitation. As the pressure is increased, the weight of this double-peak decreases, and the $f^{13} \rightarrow f^{12}$ excitation appears around 8 eV ($\approx U$) below the $f^{14} \rightarrow f^{13}$ double-peak. While the analytic continuation smears the high energy features of the CTQMC spectra, HI is known to incorrectly reduce the width of the Hubbard bands.

When the valence transition approaches completion as in the HI result (bottom of Fig. 2a), the $j = 7=2$ $f^{14} \rightarrow f^{13}$ peak overlapping the Fermi level shifts increasingly above this energy to become the unoccupied upper Hubbard band for the 4f states, corresponding to the new 4f hole. A close examination of the CTQMC counterpart (Fig. 2c), on the other hand, shows the corresponding $j = 7=2$ structure to contain a relatively large peak at the Fermi level with shoulders to either side. Based on the temperature scaling of the Fermi level peak, we believe it to be a quasiparticle or Kondo-like contribution consistent with increasing delocalization of the 4f hole as volume is reduced, and that the lower shoulders are likely of more Hubbard character. Moreover, any transfer of spectral weight into such a quasiparticle contribution at the expense of the $f^{13} \rightarrow f^{12}$ Hubbard band would also contribute to a larger DMFT (QMC) n_f than in DMFT (HI) as is observed. Finally, both the simultaneous existence of two lower Hubbard bands, and the gradual transfer of spectral weight evident in Fig. 2 are fundamental signatures of electron correlation which a single-particle approach such as LDA or LDA+U cannot reproduce.

Thus far we have shown a gradual emptying of the 4f shell with applied pressure and the corresponding changes in the single-particle spectra interpreted in terms of the relative abundance of f^{13} and f^{14} configurations in the system. We now present an analysis of the associated local charge fluctuations in Yb. In Fig. 3a we compare the local charge fluctuations in Yb, defined through the mean square deviation of the f-occupation $\langle n_f^2 \rangle$; $\hat{n}_f = \hat{n}_f - n_f$, with those in Ce, Pr and Nd [14]. While Ce, Pr and Nd show a monotonic increase of $\langle n_f^2 \rangle$ with pressure, the charge fluctuations in Yb exhibit a local maximum around 27 Å³/atom where $n_f \approx 13.5$. Evaluating the thermal expectation in a basis of n_f eigenstates yields $\langle n_f^2 \rangle = w_{13}(1 - w_{13})$, if we assume only f^{13} and f^{14} configurations have significant weight ($w_{13} + w_{14} = 1$), and thus a peak in the midst of the valence transition $w_{13} = 0.5$. On the other hand, if a single f^n configuration predominates ($w_n = 1$) but then loses weight to f^{n-1} and f^{n+1} states due to growing hybridization under compression, one will see a monotonic increase in $\langle n_f^2 \rangle$. It would appear likely that the behavior seen in Fig. 3a for Yb is reflects a combination of both effects, while that of Ce, Pr, and Nd is primarily the latter delocalization behavior.

To gain more insight we further evaluate the local charge susceptibility $\chi^{(1)}$ (Fig. 3b), obtained from the imaginary-time correlation function

$$\chi^{(1)} = \int_0^Z d\tau \langle \hat{n}_f(\tau) \hat{n}_f(0) \rangle; \quad \langle \hat{n}_f(\tau) \hat{n}_f(0) \rangle = \langle \hat{n}_f(\tau) \hat{n}_f(0) \rangle; \quad (2)$$

We find that the initial increase of the charge fluctuations with pressure is mirrored by an increase of the local charge susceptibility with both having their maxima at about the same volume, however, the increase of $\langle n_f^2 \rangle$ at high pressure is not reflected in the charge susceptibility. The origin of this behavior is revealed in the inset of Fig. 4 where we compare the imaginary time charge correlations for $V = 13.6$ and 29.0 Å³/atom. While the magnitude of the charge fluctuations is about the same ($\mu = 0$ intercepts), the fluctuations at high pressure are short lived (rapid decay with increasing τ) leading to a relatively lower susceptibility. In Fig. 4 we show the corresponding physical susceptibilities on the real frequency axis, imaginary parts of which characterizes the density of charge excitations.

$$\chi''(\omega) = \frac{1}{\omega} \int_0^Z d\tau \langle \frac{e^{-i\omega\tau} + e^{i\omega\tau}}{1 - e^{-\tau}} \rangle; \quad (2) \quad (3)$$

Comparison of $\chi''(\omega)$ and $\chi^{(1)}$ shows that slowly decaying fluctuations are, as expected, related to low energy charge excitations.

Low energy local charge excitations in strongly correlated metals are rather rare since they are usually suppressed by the onsite Coulomb repulsion, as is the case for Ce, Pr, and Nd where $T^{(1)}$ is 20–60 times smaller than $\langle n_f^2 \rangle$ over the volume range of Fig. 4b [14]. Existence of such excitations and the corresponding maxima

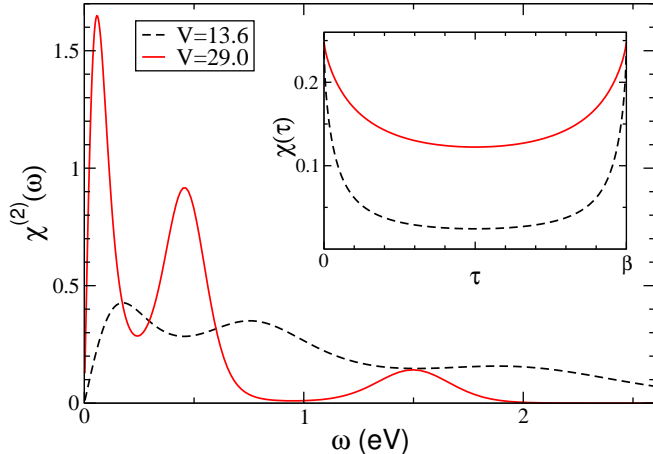


FIG. 4: (Color online) Imaginary part of the local f-f charge susceptibility at 630 K and specific volumes of 13.6 \AA^3 (black dashed line) and 29.0 \AA^3 (red solid line) per atom. The inset shows the corresponding imaginary time correlation functions obtained with CTQMC.

in ⁽¹⁾ vs V and $\hbar n_{\text{f}}^{\text{2}}$ vs V curves distinguishes this fluctuating valence behavior of Yb from the intermediate valence behavior of the other studied lanthanides. The calculated local charge susceptibility provides a clear physical meaning to the earlier reports of near degeneracy of $2+$ and $3+$ valence states in Yb [1]. There is also a direct connection to the experimental observation of the unusual pressure-volume curve of Yb, namely the compressibility of the electronic subsystem is proportional to its charge susceptibility. It is plausible to expect that the maximum of local ⁽¹⁾ vs V leads to softening of the entire electronic liquid, although the effect will be to some extent masked by the presence of spd bands.

Our local charge fluctuation and susceptibility results suggest that pressure affects metallic Yb essentially in two ways which can, to a first approximation, be looked at separately: hole doping of the filled $4f$ shell and growing hybridization of the $4f$ bands with the spd bands. In regard to the first mechanism, it is the crossover of atomic-like f^{13} and f^{14} levels which drives the valence transition creating a peak in $\hbar n_{\text{f}}^{\text{2}}$ as noted. Since the system is then also sensitive to external perturbations breaking this near degeneracy, a large charge susceptibility also follows. Hole doping into the atomic-like $4f$ shell can therefore explain both the (local) maxima in $\hbar n_{\text{f}}^{\text{2}}$ and ⁽¹⁾. The second mechanism, growing hybridization with its concomitant $4f$ delocalization, leads to an increase of charge fluctuation $\hbar n_{\text{f}}^{\text{2}}$ at higher pressures, as well as to the screening of these fluctuations, and thus the small charge susceptibility ⁽¹⁾, in analogy to screening of magnetic moment in the Anderson impurity model.

We have examined the pressure induced valence tran-

sition of elemental Yb using the LDA + DMFT approach⁴. The transition is advanced also by increasing temperature at larger volumes, and appears to have reached its trivalent limit by the smallest volumes considered, where there is evidence of Kondo-like structure in the spectra as found with the early lanthanides. Perhaps most interestingly we find that while the f orbital occupation and the single-particle spectra evolve monotonically with compression, the charge fluctuations and local charge susceptibility exhibit a distinct peak. We interpret this feature as fluctuating valence behavior in contrast to Ce, Pr and Nd which can be classified as intermediate valence systems.

The authors would like to thank Philipp Werner for providing his CTQMC code and Richard T. Scalettar and Simone Chiesa for stimulating discussions. E. R. Y. and W. E. P. were supported by DOE SciDAC Grant No. DE-FG02-06ER25794. J.K. acknowledges the support of SFB 484 of the Deutsche Forschungsgemeinschaft. Work at LLNL was performed under the auspices of the U.S. DOE under contract W-7405-ENG-48.

-
- [1] P. Strange, et al., Nature 399, 756 (1999).
 - [2] K. Held, et al., Phys. Stat. Sol. (b) 243, 2599 (2006).
 - [3] G. Kotliar, et al., Rev. Mod. Phys. 78, 865 (2006).
 - [4] M. B. Zolner, et al., Phys. Rev. Lett. 87, 276403 (2001).
 - [5] K. Held, A. K. M. Mahan, and R. T. Scalettar, Phys. Rev. Lett. 87, 276404 (2001).
 - [6] A. K. M. Mahan, K. Held, and R. T. Scalettar, Phys. Rev. B 67, 075108 (2003).
 - [7] A. K. M. Mahan, Phys. Rev. B 72, 115125 (2005).
 - [8] B. Amadon, S. Biermann, A. Georges, and F. Aryasetiawan, Phys. Rev. Lett. 96, 066402 (2006).
 - [9] J. H. Shim, K. Haule, and G. Kotliar, Science 318, 1615 (2007).
 - [10] K. Takemura and K. Syassen, J. Phys. F 15, 543 (1985).
 - [11] F. Barson, S. Legvold, and F. H. Spedding, Phys. Rev. 105, 418 (1957).
 - [12] J. E. Hirsch and R. M. Fye, Phys. Rev. Lett. 56, 2521 (1986).
 - [13] P. Werner, et al., Phys. Rev. Lett. 97, 076405 (2006).
 - [14] A. K. M. Mahan, R. T. Scalettar, and M. Jarrell, unpublished.
 - [15] K. Syassen, et al., Phys. Rev. B 26, 4745 (1982).
 - [16] C. Dallera, et al., et al., Phys. Rev. B 74, 081101(R) (2006).
 - [17] F. Reinert, et al., Phys. Rev. B 58, 12808 (1998).
 - [18] H. Sato, et al., Phys. Rev. B 69, 165101 (2004).
 - [19] S. Schmitt, S. Hufner, F. Reinert, and W. Assmus, Phys. Rev. B 71, 195110 (2005).
 - [20] J. J. Joyce, et al., Phys. Rev. B 54, 17515 (1996).
 - [21] B. P. Doyle, et al., Phys. Rev. B 75, 235109 (2007).
 - [22] R. N. Silver, D. S. Sivia, and J. E. Gubematis, Phys. Rev. B 41, 2380 (1990).